Dynamics and Predictability of Stommel's box model:

A phase space perspective with implications for decadal climate variability

Gerrit Lohmann[1]

Max-Planck-Institut für Meteorologie, Bundesstrasse 55, 20146 Hamburg, Germany

and Joachim Schneider[2]

Philipps Universität Marburg, Renthof 7, 35032 Marburg/Lahn, Germany.

Journal: Tellus

September 1998

1: corresponding author; email: gerrit.lohmann@dkrz.de

2: current affiliation: Data General Walldorf, Germany

Abstract

The dynamics and predictability of Stommel's (1961) box model of the thermohaline circulation is studied. This nonlinear model with idealized geometry of the North Atlantic is solved exactly. A phase space analysis of the model reveals that the optimal perturbation affecting long-term climate variability is provided by high latitude haline forcing in the Atlantic ocean, although this perturbation has little resemblance with the most unstable mode of the system and the leading EOF.

Furthermore, the predictability problem is investigated by means of singular vector analysis and the evolution of the probability distribution function. Uncertainties in the oceanic initial conditions do increase in the phase space of the model. In the stochastically forced box model with identical oceanic initial conditions, the climate predictability is examined for the damped persistence forecast. We find that the loss of the predictability is related to the different stages of the variance evolution which is also measured by the relative entropy. Our analysis shows that the non-normal system matrix of Stommel's model does affect the dynamics and predictability of the system which is useful for the interpretation of long-term climate variability and predictability.

1 Introduction

The oceanic thermohaline circulation (THC) occupies a central position in the understanding of climate variability and predictability because of its link to long-term variability and climate changes. In the North Atlantic, warm and saline surface water is transported northward, and on its pathway it is cooled and freshened through surface fluxes. The large amount of heat transported by the THC is responsible for the relatively mild climate in northern Europe. Most of the northward oceanic heat transport is associated with the meridional overturning which is driven, at least in part, by deep water formation in the Labrador and Nordic Seas.

The pioneering work of Stommel (1961) demonstrated the existence of multiple equilibria under same atmospheric forcing conditions. Stommel's result with an ocean box model has initiated studies using three dimensional ocean circulation models (Bryan, 1986; Manabe and Stouffer, 1988), confirming the existence of multiple equilibria. Besides the modeling studies, there is paleoclimatic evidence (e.g. Lehmann and Keigwin, 1982) that secular variability and abrupt climate changes are linked to variations in the THC. In addition to paleoclimatic shifts, interdecadal climate variability may originate from changes of North Atlantic Deep Water (NADW) formation. A large salinity fluctuation in the northern North Atlantic was observed in the early seventies, known as the "Great Salinity Anomaly" (Dickson et al., 1988) which temporarily weakened deep water formation in the Labrador Sea (Lazier, 1988).

We present in this paper the analytical solution of Stommel's (1961) low order model. The model mimics the North Atlantic region which seems to be a very sensitive part of the global thermohaline circulation. With a coupled atmosphere-ocean version of this model, we analyze the qualitative behavior of the THC in terms of stability, variability, and predictability. The model dynamics are analyzed in phase space and we examine the most effective excitation of the model variability.

The issue of atmospheric predictability started with the work of Lorenz (1965). This was later extented to a coupled atmosphere-ocean mixed layer model (Nese and Dutton, 1993). Although the typical predictability limit of weather phenomena is of the order of weeks, climate variations are much more predictable due to the large oceanic heat capacity and dynamical inertia. Other modeling studies deal with the forecast of the dominant interannual climate fluctuation, the El Niño/Southern Oscillation (Goswami and Shukla, 1991; Blumenthal, 1991; Eckert and Latif, 1997). For the North Atlantic, the predictability should include an active THC which was recently addressed by Griffies and Bryan (1997). In several predictability experiments with their complex coupled model, they estimated the predictability of the dominant EOF patterns. They concluded that the ocean-atmosphere interactions yield to predictability limits beyond the intrinsic predictability limits of the atmosphere. Following their approach, we will address the question of predictability in our simple model which is forced by stochastic atmospheric white noise stemming from the underlying dynamical processes in the atmosphere.

The paper is organized as follows:
We present the exact solution of Stommel's (1961) box model (section 2). In section 3, the dynamics and error growth is analyzed in the phase space of the model. A stochastically forced box model is presented in section 4. We are particularly interested in the type of forcing which leads to maximal long-term variability and predictability. The damped persistence forecast and a concept adapted from information theory are applied to our model. The results are discussed and conclusions are given in section 5.

2 Solution of Stommel's model

In this section, a category of the nonlinear models following the simple thermohaline model of Stommel (1961) is solved exactly. The common assumption of these box

models is that the oceanic overturning rate Φ can be expressed by the meridional density difference:

$$\Phi = -c\,(\alpha \Delta T - \beta \Delta S) \qquad , \tag{1}$$

where α and β are the thermal and haline expansion coefficients, c is a tunable parameter, and Δ denotes the meridional difference operator. Stommel (1961) considered a two-box ocean model where the boxes are connected by an overflow at the top and a capillary tube at the bottom, such that the capillary flow is directed from the high density vessel to the low density vessel following the law (1).

The equations for temperature T and salinity S are the heat and salt budgets in one oceanic box using an upstream scheme for the advective transport:

$$\frac{d}{dt}T = - \frac{\Phi}{V}\Delta T - \frac{F_{oa}}{\rho_0 c_p h} \tag{2}$$

$$\frac{d}{dt}S = - \frac{\Phi}{V}\Delta S - \frac{S_0}{h}(P-E) \qquad , \tag{3}$$

where V is the volume of the box with depth h, and $(P-E)$ denotes the fresh water flux (precipitation minus evaporation plus runoff). F_{oa} is the heat flux at the ocean-atmosphere interface, S_0 is a reference salinity, and $\rho_0 c_p$ denotes the heat capacity of the ocean. For simplicity, we have restricted our notation to the case with high latitude deep water formation. For a reversed circulation, the parameter c in (1) must then be substituted by $-c$.

The budget equations for temperature and salinity (2, 3) for each box with volume V can be subtracted from each other in order to get:

$$\frac{d}{dt}\Delta T = - 2\,\frac{\Phi}{V}\Delta T - \Delta\,\frac{F_{oa}}{\rho_0 c_p h} \tag{4}$$

$$\frac{d}{dt}\Delta S = - 2\,\frac{\Phi}{V}\Delta S - \Delta\,\frac{S_0}{h}(P-E) \qquad . \tag{5}$$

As in Lohmann et al. (1996), we assume a linear response model for the surface fluxes F_{oa} and $P-E$ as function of sea surface temperature (Appendix A.1). The

equilibrium temperature and salinity gradients $(\Delta T^\circ, \Delta S^\circ)$ correspond to those values for which the left hand side of (4) and (5) vanish. The resulting cubic function for ΔT° in terms of ΔS° has three real solutions for a wide range of parameters in the model (Stommel, 1961).

We subtract the climatic background state $(\Delta T^\circ, \Delta S^\circ)$ from the dynamical equations (4, 5) resulting a nonlinear evolution equations for the anomalies $\Delta T - \Delta T^\circ$ and $\Delta S - \Delta S^\circ$ which are denoted in the following by T and S, respectively. Denoting[1] furthermore $\boldsymbol{X}$ for the two dimensional vector (T, S), the evolution equation for the anomalies T and S is of the following structure:

$$\frac{d}{dt}\boldsymbol{X} \;=\; \boldsymbol{A}\boldsymbol{X} \;+\; \langle\, \boldsymbol{b} | \boldsymbol{X} \,\rangle \;\; \boldsymbol{X}\,, \qquad \boldsymbol{X}(0) = \boldsymbol{X}_0 \quad \text{for} \quad \boldsymbol{X}, \boldsymbol{X}_0 \in \mathsf{R}^n, n \in \mathsf{N}\,. \tag{6}$$

The brackets $\langle \mid \rangle$ denote the Euclidean scalar product. This evolution equation (6) without inhomogeneities has the stationary solution $\boldsymbol{X} = \boldsymbol{0}$, corresponding to the stationary state $(\Delta T^\circ, \Delta S^\circ)$. In the Appendix A.1, matrix $\boldsymbol{A}$ and vector $\boldsymbol{b}$ are specified for the box model.

Let $\boldsymbol{\xi} \in \mathsf{R}^n$ denote the solution of

$$\boldsymbol{A}^* \boldsymbol{\xi} \;+\; \boldsymbol{b} \;=\; \boldsymbol{0} \qquad , \tag{7}$$

where $\boldsymbol{A}^*$ is the adjoint operator to $\boldsymbol{A}$. With the definition

$$\boldsymbol{X}(t) \;:=\; \frac{1}{\gamma(t)} \;\exp(\boldsymbol{A}t)\, \boldsymbol{X}_0\;, \qquad \boldsymbol{X}_0, \boldsymbol{X}(t) \in \mathsf{R}^n \tag{8}$$

and the scaling function

$$\gamma(t; \boldsymbol{X}_0) \;:=\; \langle\, \boldsymbol{\xi} \,|\, \exp(\boldsymbol{A}t)\boldsymbol{X}_0 \,\rangle \;-\; \langle\, \boldsymbol{\xi} | \boldsymbol{X}_0 \,\rangle \;+\; 1 \qquad , \tag{9}$$

one can verify that $\boldsymbol{X}(t)$ of (8) solves the differential equation (6):

$$\begin{aligned} \frac{d}{dt}\boldsymbol{X} \;&=\; \boldsymbol{A}\,\frac{1}{\gamma}\exp(\boldsymbol{A}t)\boldsymbol{X}_0 \;-\; \frac{\dot\gamma}{\gamma^2}\exp(\boldsymbol{A}t)\boldsymbol{X}_0 \\ &=\; \boldsymbol{A}\boldsymbol{X} - \langle \boldsymbol{\xi} | \boldsymbol{A}\boldsymbol{X} \rangle \;\; \boldsymbol{X} \;=\; \boldsymbol{A}\boldsymbol{X} + \langle \boldsymbol{b} | \boldsymbol{X} \rangle \;\; \boldsymbol{X} \quad . \end{aligned} \tag{10}$$

[1] Bold face is used for vectors and matrices throughout the paper

The models of Stommel (1961), Marotzke and Stone (1995), Lohmann et al. (1996), Ruddick and Zhang (1996), Winton (1997) and many others are of type (6), and their dynamics are therefore exactly known.

3 Dynamics and error growth

In this section, we analyze the sensitivity of the model and its variability in phase space. In particular, we examine why salinity perturbations are so important in changing the THC, and how errors in the initial conditions develop further.

3.1 Dynamics

The model is tuned to the present climate (Lohmann et al., 1996) which places it in the thermal regime of the THC with a meridional overturning rate Φ° of $14\,Sv$ ($1\,Sv = 10^6 m^3 s^{-1}$). We seek the initial conditions for which $\boldsymbol{X}(t)$ asymptotically reaches this equilibrium state. Because $\gamma = 1$ initially (9), this question can be reduced to the determination of initial conditions $\boldsymbol{X}_0$ where $\gamma(t; \boldsymbol{X}_0) > 0$ is positive for all $t \geq 0$. The grey area in the phase space spanned by temperature and salinity (Fig.1) indicates the region of unstable initial states which are outside the basin of attraction for the thermally driven THC. The circulation with North Atlantic Deep Water formation is possible only in the white area (Fig.1), basic states with a large meridional salinity or small temperature gradient are not stable. Furthermore, we find that the critical perturbation is mainly a function of the strength of the background meridional mass transport Φ° (not shown).

We analyze the dynamics in the phase space spanned by temperature and salinity anomalies and investigate the model sensitivity under anomalous high latitude forcing, induced as an initial perturbation. The lines in Fig.1 are phase space trajectories after perturbations of different magnitude have been injected into the North Atlantic. We notice that for most trajectories, the distances from zero $(0, 0)$ in-

creases temporarily, where the maximal distance from zero is after a decade. After about 10 years the trajectories in Fig.1 point into a "mixed temperature/salinity direction", denoted further as e_1. Fig.1 imply that the adjustment of the THC involves two phases: A fast thermal response and a slower response on the e_1-direction. We shall see later that the vector $\boldsymbol{e}_1$ is identical with the most unstable mode in the system. Because the scaling function $\gamma(t)$ acts upon both temperature and salinity (equation 8), the evolution of the nonlinear model can be well characterized by the eigenvectors of the matrix $\boldsymbol{A}$, which is discussed in the next section.

3.2 Initial excitation

The operator $\boldsymbol{A}$ of the box model is found to be non-normal $(\boldsymbol{A}\boldsymbol{A}^* \neq \boldsymbol{A}^*\boldsymbol{A})$, and the eigenvectors of $\boldsymbol{A}$, $\boldsymbol{e}_1$ and $\boldsymbol{e}_2$, are not orthogonal (Fig.2). One eigenvalue ($\boldsymbol{e}_2$) is closely related to temperature anomalies, whereas the other ($\boldsymbol{e}_1$) is a "mixed temperature/salinity eigenvector" (Fig. 2). The eigenvectors of the adjoint matrix $\boldsymbol{A}^*$ are denoted by $\boldsymbol{e}_1^*$ and $\boldsymbol{e}_2^*$, respectively. For the non-normal matrix $\boldsymbol{A}$, the eigenvectors of $\boldsymbol{A}$ and $\boldsymbol{A}^*$ do not coincide, but fulfilling the "biorthogonality condition": $\boldsymbol{e}_1^* \perp \boldsymbol{e}_2$ and $\boldsymbol{e}_2^* \perp \boldsymbol{e}_1$. For the linear dynamics $\gamma\boldsymbol{X}$, we make the ansatz

$$\gamma\,\boldsymbol{X} \quad = \quad c_1\;\boldsymbol{e}_1\;\exp(\lambda_1 t) \;+\; c_2\;\boldsymbol{e}_2\;\exp(\lambda_2 t) \qquad , \tag{11}$$

where the eigenvalues $\lambda_{1,2}$ correspond to the eigenvectors $\boldsymbol{e}_{1,2}$. In our system, both eigenvalues are real and negative. Because of $\lambda_2 < \lambda_1$, the first term dominates for long time-scales and the second for short time scales. Using the biorthogonality condition, we get furthermore the coefficients

$$c_i \;=\; \frac{\langle \boldsymbol{e}_i^* | \boldsymbol{X}_0 \rangle}{\langle \boldsymbol{e}_i^* | \boldsymbol{e}_i \rangle} \qquad \text{for} \quad i = 1, 2 \quad . \tag{12}$$

A perturbation is called "optimal", if the initial error vector has minimal projection onto the subspace with fastest decaying perturbations, or equivalently if the coefficient c_1 is maximal. This is according to (12) equivalent to $\boldsymbol{X}_0$ pointing

into the direction of $\boldsymbol{e}_1^*$. This unit vector $\boldsymbol{e}_1^*$ is called the "biorthogonal" (Palmer, 1996) to the most unstable eigenvector $\boldsymbol{e}_1$ which we want to excite.[2] The most unstable mode $\boldsymbol{e}_1$ and its biorthogonal $\boldsymbol{e}_1^*$ differ greatly from each other, and the perturbation that optimally excites the mode bears little resemblance to the mode itself.

It is remarkable that the optimal initial perturbation vector $\boldsymbol{e}_1^*$ does not coincide with a perturbation in sea surface density at high latitudes, which would reside on the dotted line perpendicular to $\rho = const.$ in Fig.2. Even when using a space spanned by $(\alpha T, \beta S)$ instead of (T, S), to take into account the different values for the thermal and haline expansion coefficients, vector $\boldsymbol{e}_1^*$ is much more dominated by the scaled salinity anomalies than the temperature anomalies of the high latitudinal box.[3]

3.3 The error growth due to uncertain initial conditions

Assume that the oceanic initial conditions of our model are uncertain which could be due to the lack of exact measurements or due to extreme events. Our interest is in identifying and analyzing which uncertainties in the initial conditions are crucial for the limitation of the system's predictability. In our box model, the evolution $\boldsymbol{X}(t)$ is known. Thus, the tangent linear operator $\boldsymbol{A}(\boldsymbol{X})$ can be obtained analytically. The evolution on the tangent vector space is given by: $\boldsymbol{x}(t) = \exp(\boldsymbol{A}t)\ \boldsymbol{x}_0$ and the growth of the error vector $\boldsymbol{x}(t)$ can be measured by the norm of the symmetric

[2] In order to make a geometrical picture for the mathematical considerations, assume that the tail of the vector $\boldsymbol{X}_0$ is placed on the $\boldsymbol{e}_1-$line and its tip on the $\boldsymbol{e}_2-$line. This vector is stretched maximally because the tail decays to zero quickly, whereas the tip is hardly unchanged due to the larger eigenvalue λ_1.

[3] We have chosen the (T, S)-space instead of $(\alpha T, \beta S)$, in order to make the phase space analogy more clear and to discuss the effect of changed α under different climatic conditions. For colder climate states, the angle between the eigenmodes $\boldsymbol{e}_1$ and $\boldsymbol{e}_2$ decreases and the transient amplification in Fig.1 is stronger.

matrix $e^{\boldsymbol{A}^* t}\, e^{\boldsymbol{A} t}$:

$$||\boldsymbol{x}(t)||^2 \quad := \quad \left\langle e^{\boldsymbol{A} t}\boldsymbol{x}_0 \,|\, e^{\boldsymbol{A} t}\boldsymbol{x}_0 \right\rangle \quad = \quad \left\langle e^{\boldsymbol{A}^* t} e^{\boldsymbol{A} t}\, \boldsymbol{x}_0 | \boldsymbol{x}_0 \right\rangle \qquad . \tag{13}$$

The eigenvectors of the so-called Oseldec-operator $e^{\boldsymbol{A}^* t}\, e^{\boldsymbol{A} t}$ are the singular vectors of the tangent linear operator $\boldsymbol{A}$. The eigenvalues of $e^{\boldsymbol{A}^* t}\, e^{\boldsymbol{A} t}$ are connected to the amplification rates of $\boldsymbol{x}(t)$.

We suppose that the initial conditions are uncertain and are normally distributed in phase space. The initial state is then represented by a circle in phase space (Fig.3) where the axis units correspond to the same density contribution. The development for five different times 1 day, 1 month, 6 months, 1 year, and 2 years is shown in Fig.3. For time-scales larger than 2 years, the ellipsoids coincide almost with a line on the major axis are therefore not shown in Fig.3. The initial circle is stretched during the evolution, thereby decreasing its area by the factors $0.99, 0.89, 0.50, 0.25,$ and 0.06 , respectively. The main axes of the ellipsoids define the singular vectors of the system. The forecast ellipsoids rotate further in phase space (Fig.3). Initially, $e^{\boldsymbol{A}^* t}\, e^{\boldsymbol{A} t}$ can be approximated by $\mathbf{1} + (\boldsymbol{A}^* + \boldsymbol{A})\, t$, and the ellipsoid deformation for initial time coincides with the vector $(\boldsymbol{e}_1 + \boldsymbol{e}_1^*)/2$ (Fig.2). After a few months, the error growth is rotated into the direction of the next term of the Taylor expansion $(\, \boldsymbol{A}^* \boldsymbol{A}\, t^2/2\,)$ of the Oseldec-operator. After one year, the dominant singular vector coincides almost with sea surface salinity anomalies. We obtain that ellipsoids after a few years degenerate to a line, and asymptotically they are reduced to the origin $(0, 0)$ because the matrix $\boldsymbol{A}$ is asymptotically stable.

It follows that errors in high latitude sea surface temperature (SST) are less important in the initial conditions than sea surface salinities when predicting the evolution of oceanic variables. We find that a negative feedback (damping) of SST-anomalies in the northern North Atlantic due to the atmospheric response model is essential for our conclusions. A positive feedback for SST-anomalies would amplify

initial errors, making the SST highly unpredictable. We find furthermore that the dominant error growth vector changes only slightly for different background climatic states $(\Delta T^\circ, \Delta S^\circ)$ and thus for a whole model trajectory $\boldsymbol{X}(t) = (T(t), S(t))$.

4 The stochastically forced box model

We generalize Stommel's (1961) dynamics (4, 5) to the stochastically driven system where additive noise in the temperature and salinity dynamics reflects the variance of heat and freshwater fluxes due to synoptic activity (Hasselmann, 1976; Lemke, 1977). We consider moderate stochastic forcing only, and a numerical simulation of the stochastic differential equation shows that the nonlinear terms in the stochastic differential equation play a minor role. For simplicity, the linearized version is discussed only. With the abbreviation $X_1 = T$ and $X_2 = S$ as in the previous sections, this set of equations can be rewritten as

$$\frac{d}{dt}\boldsymbol{X} \quad = \quad \boldsymbol{A}\,\boldsymbol{X} \; + \boldsymbol{F}\,\boldsymbol{\eta} \quad , \qquad \boldsymbol{X}, \boldsymbol{\eta} \in \mathsf{R}^2 \tag{14}$$

with $\boldsymbol{\eta}(t)$ as a white noise forcing with unit variance and zero mean, and $\boldsymbol{F}$ as a matrix specified later. The solution of this linear stochastic differential equation is the stochastic integral

$$\boldsymbol{X}(t) \quad = \quad e^{\boldsymbol{A}t}\,\boldsymbol{X}_0 \quad + \quad e^{\boldsymbol{A}t}\int_o^t e^{-\boldsymbol{A}s}\,\boldsymbol{F}\,\boldsymbol{\eta}(s)\,ds \qquad . \tag{15}$$

4.1 Stochastic excitation

In the previous sections 3.2 and 3.3, we have investigated at the sensitivity of the THC with respect to initial conditions. Here, we want to consider the statistical steady state, and to seek that stochastic forcing F which most effectively excites the stationary variance. From (15), the variance induced by the stochastic forcing is

$$E\,\left\{(\boldsymbol{X}-\bar{\boldsymbol{X}})^2\right\} \; = Tr\left[\,\boldsymbol{F}^*\,\left(\int_o^t e^{\boldsymbol{A}^*(t-s)}\,e^{\boldsymbol{A}(t-s)}ds\right)\,\boldsymbol{F}\,\right] =: \, Tr\,[\,\boldsymbol{F}^*\,\boldsymbol{B}_t\,\boldsymbol{F}\,] \tag{16}$$

with the positive hermitian $\boldsymbol{B}_t$ accumulating the perturbation growth. The variance (16) is maximal, if the matrix $\boldsymbol{F}$ consists of the eigenvectors of $\boldsymbol{B}_t$, because then the matrix $\boldsymbol{F}^* \boldsymbol{B}_t \boldsymbol{F}$ has diagonal form and the trace in (16) is maximal.

Because the matrix $\boldsymbol{A}$ is asymptotically stable, the statistics are stationary. For the statistically steady state, the eigenvectors of $\boldsymbol{B}_\infty = \lim_{t\to\infty} \boldsymbol{B}_t$ are ordered according to their contribution to the variance and are called "stochastic optimals" (Farrell and Ioannou, 1996) for the linearized dynamics (14). The leading stochastic optimal (shown as *so*1 in Fig.4), excites most effectively the stationary variance. This vector points almost into the direction of the most efficient excitation vector $\boldsymbol{e}_1^*$ (Fig.4). The effective span of the variance is referred as to the empirical orthogonal functions (EOFs). The first EOF (eof1 in Fig.4), explaining more than 99% of the total variance, is quite different from the vector which most effectively excites the stationary variance (so1) which is a common feature of non-normal systems (Farrell and Ioannou, 1996).

4.2 Predictability

In this section, we use the additive stochastic forcing components in (14) with equal contributions to the high latitude density such that the variances of αT and βS have the same magnitude in (14). We define the ensemble mean vector $\bar{\boldsymbol{X}} = (E\{\boldsymbol{X}_i\})$ and the covariance matrix $\boldsymbol{R} = (\boldsymbol{R}_{ij}) = \left(E\{(\boldsymbol{X}_i - \bar{\boldsymbol{X}}_i)(\boldsymbol{X}_j - \bar{\boldsymbol{X}}_j)\}\right)$. In the statistically steady state, the eigenvectors of the asymptotic variance matrix $\boldsymbol{R}_\infty = \lim_{t\to\infty} \boldsymbol{R}_{ij}$ span the maintained variance (EOFs. The leading EOF (eof1 in Fig.4) is the first eigenvector of $\boldsymbol{R}_\infty$. One can prove that the time evolution of the covariance matrix $\boldsymbol{R}(t)$ is given by

$$\boldsymbol{R}(t) \quad = \quad \boldsymbol{R}_\infty \; - \; e^{\boldsymbol{A}t} \; \boldsymbol{R}_\infty \; e^{\boldsymbol{A}^* t} \quad . \tag{17}$$

The matrix $\boldsymbol{R}(t)$ is symmetric and its eigenvectors rotate in phase space, which is a consequence of the non-normal evolution operator $\boldsymbol{A}$. The solution (15) corresponds to the solution of a Fokker-Planck equation, an evolution equation for the probability distribution function (Appendix A.2). Starting with a $\delta-$function at initial time (and assume without loss of generality zero mean), the time evolution of the probability distribution functions (PDFs) is shown in Fig.5. In a system where the eigenvector would be orthogonal, the PDF would not rotate because the dynamics can be reduced to statistically independent normal modes.

The mean square difference between the realizations $\boldsymbol{X}(t)$ and the mean vector $\bar{\boldsymbol{X}}(t)$ provides a definition of the error in the forecast and is called damped persistence forecast of the ensemble mean $\bar{\boldsymbol{X}}$ (Lorenz, 1973). The loss of predictability in the first year is largest for salinity (Fig.5 a and b), and after 2 years, the variance is greatest in the direction of the first EOF (Fig.5 c and d).

Assuming an initial anomaly $\boldsymbol{X}_0$, a net skill parameter of climate prediction may be defined by the signal to noise ratio. A more objective way to define predictability is in the framework of information theory (Leung and North, 1990). This concept makes use of an ensemble entropy $E(t)$ which yields a predictability measure for the evolution.[4] Fig.6 shows the negative of the relative entropy which decreases in time. This quantity is also called transinformation, and the values of $-E(t)$ can be associated with the amount of uncertainty, which can be removed if we know the initial anomaly (Leung and North, 1990). The decay of $-E(t)$ in Fig.6 corresponds to different dynamical stages of our two dimensional problem. In the first month, the information loss is mainly due to the broadening of the PDF in the salinity direction (corresponding to Fig.5 a). After that time, the rms error increases with a larger e-folding time, and the knowledge about the system is very small after a decade (Fig.6). The stationary PDF has maximal variance and contains therefore

[4]For a detailed definition and calculation of $E(t)$, we refer to the Appendix A.2

less information about the system. The loss of predictability can also be associated with the overlap of the actual PDF with the stationary PDF (Eckert and Latif, 1997).

5 Discussion and Conclusions

We have presented an analytical solution for the types of models proposed by Stommel (1961). This box model, consisting of the components to the meridional buoyancy gradient in the North Atlantic ocean, has been used as a paradigm for multiple equilibria of the large-scale ocean circulation. Starting from the analytical solution of Stommel's model, we found a class of exactly solvable nonlinear differential equations. Interestingly, this class of differential equations form singularities and the dynamics has a finite escape time. The explicit solution of the Stommel (1961) box model enables us to study the parameter sensitivity, dynamics, and error growth of this idealized model of the thermohaline circulation. We have focussed mainly on aspects of the model phase space spanned by temperature and salinity and on its consequences for long-term climate variability.

Our results suggest that climatic states which are associated with NADW formation are located in a specific part of the phase space only where the NADW circulation with a large meridional salinity or small temperature gradient is not stable. This is also supported by the recent coupled GCM experiments of Tzipermann (1997) who finds inherently unstable climate behavior due to weak THC.

Because of the special structure of the analytical solution, the dynamics can be traced by the eigenvectors in phase space which are found to be highly non-orthogonal. In the model phase space, we found that the temperature response is very fast compared to that of the most unstable mode. The most unstable mode represents a mixed temperature/salinity vector. Applying the concept of Farrell and

Ioannou (1996) to the non-normal system matrix of Stommel's model of the North Atlantic, it is retrieved that haline perturbations in the northern North Atlantic provide the most effective excitate-mechanism to the thermohaline circulation. The optimal perturbation for the model's THC, understood in terms of an initial value problem, is not due to high latitude density. The optimal perturbation is perpendicular to the temperature eigenmode of the system and has little resemblance with the most unstable mode and the leading EOF. Our study suggests that a proper conceptual model with an active THC variability should not be one-dimensional since two different regimes are coupled due to an active THC. In one-dimensional models, the stochastic optimal, the optimal excitation vector and the most unstable normal mode coincide with each other.

Furthermore, we find that the leading EOF, a mixed temperature/salinity vector, is optimally excited by salinity fluctuations in the northern North Atlantic induced by the weather noise. With our low order model, we can show that freshwater flux fluctuations play thus an important role influencing long-term climate variability. Several studies analyzed the long-term variability using stochastic upper boundary conditions. Mikolajewicz and Maier-Reimer (1990) and Weisse et al. (1994) used an ocean general circulation model under mixed boundary conditions with superimposed white noise forcing in the freshwater flux, finding a strong secular mode of variability. Other studies using models with different levels of complexity (as e.g. Griffies and Tzipermann, 1995) find also that the long-term variability depends strongly on the noise level of atmospheric fluxes. In terms of our terminology, their models are forced by perturbations that are close to the leading stochastic optimal for long-term variability.

We address the question of climate predictability in our low order model adopting the concepts of error growth dynamics and the PDF evolution. Uncertainties in the oceanic initial conditions grow in the phase space of the box model. The dominant

error growth vector rotates in the phase space and after one year, this vector is closely related to the salinity anomalies. Uncertainties in high latitude salinity are responsible for the short-term amplification of the forecast ellipsoid, because haline anomalies provide an effective instability mechanism for the THC. When modeling climate variations on decadal time-scales, the initialization of sea surface salinity is therefore more important than errors in the initial temperature field.

In our consideration of the long-term variability in the North Atlantic, we added noise to the deterministic Stommel (1961) model. The stochastic component accounts for an active participation of the THC variability, integrating short term weather fluctuations. This is consistent with the red-noise hypothesis and the role of negative feedback process in limiting climate variability (Hasselmann, 1976). In addition to the usual red-noise response, the low-frequency variability for the multivariate process is strongly enhanced due to the non-orthogonality of our system eigenvectors. Formally, the change in meridional overturning is responsible for the non-normality of the system and the coupling of temperature and salinity in the model. The modes interact such that the ensemble response variance is larger than the summation of two different autoregressive processes for the distinct time-regimes (Farrell and Ioannou, 1996). Therefore, local linear stochastic theory may not explain sea surface temperature and salinity variability when an active meridional overturning is involved in the dynamics which is consistent with Hall and Manabe's (1997) findings in a coupled GCM.

In the stochastically forced model, the prediction is traced by the probability distribution function of the corresponding Fokker-Planck-Equation. The predictability has been calculated as a damped persistence forecast (Lorenz, 1973) for the multivariate process. The response of the system to an external forcing by noise is different from the error growth dynamic conducted by the singular vector analysis. The PDF-prediction is by construction not sensitive to initial conditions, because the

initial conditions are exactly known (ideally a $\delta-$function). Our stochastic approach provides a means of quantifying the growth of the variance in time. The evolution of the probability distribution function is largely affected by the non-normality of the model, and the PDF maxima rotate in phase space. We show furthermore that the prediction skill can be quantified by the relative entropy, a measure of information in the dynamical system (Leung and North, 1990), yielding an objective criterium for the loss of predictability in the model. We argue that predictability is connected with the instabilities of the system. Using a model with much more degrees of freedom and further instability mechanisms, the ensemble experiments of Griffies and Bryan (1997) show that sea surface temperature is only predictable for a few years due to the overlying atmospheric variability. Additionally, their system is hardly predictable in regions of active convection, since convective activity provides a source of ensemble variance growth in their model with identical oceanic initial conditions.

Although the Stommel (1961) box model hardly represents the real climate system, this model is good prototype models to understand climate variability and predictability in the Atlantic area. Our analysis demonstrates that the non-normal properties of the model have a strong influence on the dynamics and predictability. Because non-normal system matrices are a quite general feature of fluid dynamical systems (Reddy, 1993; Trefethen et al., 1993), we think that more complex models could benefit from a phase space approach applied here.

Acknowledgements

M. Latif, A. Timmermann, R. Gerdes, C. Eckert, E. Maier-Reimer, and K. Rogers are gratefully acknowledged for their improvements to the manuscript. We thank Prof. Dr. K. Hasselmann and Prof. Dr. W. Maaß for their support. This work was partly supported by the Bundesministrium für Forschung und Technologie through WOCE project.

Appendix A

A.1 System matrix and exact solution

In our formulation (6), the system matrix $\boldsymbol{A}$ is specified to be:

$$\boldsymbol{A} = \begin{pmatrix} -\Phi^\circ/V + c\alpha\Delta T^\circ/V + q & -c\beta\Delta T^\circ/V \\ c\alpha\Delta S^\circ/V + p & -\Phi^\circ/V - c\beta\Delta S^\circ/V \end{pmatrix} \tag{18}$$

and vector $\boldsymbol{b}$ is $(c\alpha/V,\ -c\beta/V)$. The abbreviations for p and q are

$$p = \frac{\partial(P-E)}{\partial T} \cdot S_0/h \tag{19}$$

$$q = \frac{\partial F_{oa}}{\partial T} \cdot V/(\rho_0 c_p h) \quad . \tag{20}$$

These parameters are defined through the atmospheric response model where the meridional transports are parameterized as diffusion (Lohmann et al., 1996).

The dynamics of the model is exactly known, when the vector $\boldsymbol{\xi} = -\,(\boldsymbol{A}^*)^{-1}\ \boldsymbol{b}$ of equation (7) is specified:

$$\boldsymbol{\xi} = \frac{\begin{pmatrix} c\alpha\Phi^\circ - c\beta\, V\, p \\ c\beta\Phi^\circ - c\beta q \end{pmatrix}}{-2\Phi^\circ\Phi^\circ - q\ (c\alpha\Delta T^\circ - 2c\beta\,\Delta S^\circ)\ - c\beta V p\,\Delta T^\circ} \quad . \tag{21}$$

The denominator in (21) is the negative determinant of matrix $\boldsymbol{A}$. The units of vector $\boldsymbol{\xi} = (\xi_1, \xi_2)$ are $1/K$ and $1/psu$, respectively.

A.2 Fokker-Planck equation and entropy function

The Fokker-Planck equation which corresponds to the stochastic differential equation (14) is a partial differential equation for the probability distribution function:

$$\partial_t P(\boldsymbol{X},t) \;=\; -\nabla\cdot[\boldsymbol{A}\boldsymbol{X}\;P(\boldsymbol{X},t)] + \nabla\cdot[\boldsymbol{F}\,\boldsymbol{F}^{*}\;\nabla P(\boldsymbol{X},t)] \quad . \tag{22}$$

The solution is

$$P(\boldsymbol{X},t) = \left[\frac{det\,\boldsymbol{R}^{-1}}{(2\pi)^n}\right]^{1/2} \cdot\; \exp\left[-\frac{1}{2}\,(\boldsymbol{X}-\bar{\boldsymbol{X}})\,\boldsymbol{R}^{-1}\,(\boldsymbol{X}-\bar{\boldsymbol{X}})\right] \quad , \tag{23}$$

where $\bar{\boldsymbol{X}}(t)$ and $\boldsymbol{R}(t)$ are the ensemble mean vector and covariance matrix of (14), respectively. The stationary probability distribution function $P^{stat}(\boldsymbol{X})$ can be retrieved from (23) by replacing $\boldsymbol{R}$ by $\boldsymbol{R}_\infty$ and $\bar{\boldsymbol{X}}$ by zero.

We define the relative entropy by

$$E(t) := -\int_{\mathsf{R}^n} d\boldsymbol{X} \quad P(\boldsymbol{X},t) \quad \ln\left[\,P(\boldsymbol{X},t)\,/\,P^{stat}(\boldsymbol{X})\,\right] \tag{24}$$

and find that $E(t)$ increases monotonically in time and approaches zero for $t\to\infty$. This can be found by inserting the Fokker-Planck equation (22) into (24) or directly by calculating $E(t)$ with the solution (23):

$$E(t) \;=\; \frac{1}{2}\ln[det(\boldsymbol{R}_\infty^{-1}\boldsymbol{R})] \;-\; \frac{1}{2}\,\bar{\boldsymbol{X}}\,\boldsymbol{R}_\infty^{-1}\bar{\boldsymbol{X}} \;+\; \frac{1}{2}\,Tr[\boldsymbol{R}_\infty^{-1}e^{\boldsymbol{A}t}\boldsymbol{R}_\infty e^{\boldsymbol{A}^{*}t}] \quad . \tag{25}$$

In addition, the relative entropy is averaged over the initial state such that the second term in (25) vanishes and the function becomes independent on initial state.

References

Blumenthal, B., 1991: Predictability of a coupled ocean-atmosphere model. *J. Climate* **4,** 766-784.

Bryan, F., 1986: High latitude salinity effects and inter hemispheric thermohaline circulations. *Nature* **323,** 301-304.

Dickson, R.R., Meincke, J., Malmberg, S.A., and Lee, A.J., 1988: The "Great Salinity Anomaly" in the northern Atlantic 1968-1982. *Prog. Ocean.* **20,** 103-151.

Eckert, C., and Latif, M., 1997: Predictability of a stochastically forced hybrid coupled model of El Niño. *J. Climate* **10**, 1488-1504.

Farrell, B.F., and Ioannou, P.J., 1996: Generalized stability theory. Part I: Autonomous operators. *J. Atm. Sci.* **53**, 2025-2040.

Goswami, B.N., and Shukla, J., 1991: Predictability of a coupled ocean-atmosphere model. *J. Climate* **4,** 3-22.

Griffies, S.M., and Tzipermann, E., 1995: A linear thermohaline oscillator driven by stochastic atmospheric forcing. *J. Climate* **8,** 2440-2453.

Griffies, S.M., and Bryan, K., 1997: A Predictability Study of Simulated North Atlantic Multidecadal Variability. *Climate Dyn.* **13,** 459-487.

Hall, A., and Manabe, S., 1997: Can local linear stochastic theory explain sea surface temperature and salinity variability ? *Climate Dyn.* **13,** 167-180.

Hasselmann, K., 1976: Stochastic climate models, Part 1, Theory. *Tellus* **28,** 289-485.

Lazier, J.R.N., 1988: Temperature and salinity changes in the deep Labrador Sea, 1962-1986. *Deep-Sea Res.* **35,** 1247-1253.

Lehmann, S.J., and Keigwin, L.D.,1982: Sudden changes in North Atlantic circulation during the last deglaciation. *Nature* **356,** 757-762.

Lemke, P., 1977: Stochastic climate models, Part 3, Application to zonally averaged energy models. *Tellus* **29,** 385-392.

Leung, L.Y., and North, G.R., 1990: Information theory and climate prediction. *J. Climate* **3**, 5-14.

Lohmann, G., Gerdes, R., and Chen, D., 1996: Stability of the thermohaline circulation in a simple coupled model. *Tellus* **48 A,** 465-476.

Lorenz, E.N., 1965: A study of the predictability of a 28-variable atmospheric model. *Tellus* **7,** 157-167.

Lorenz, E.N., 1973: On the existence of extended range predictability. *J. Appl. Meteorol.* **12,** 543-564.

Manabe, S., and Stouffer, R.J., 1988: Two stable equilibria of a coupled ocean-atmosphere model. *J. Climate* **1,** 841-863.

Marotzke, J. and Stone, P.H., 1995: Atmospheric transports, the thermohaline circulation, and flux adjustments in a simple coupled model. *J. Phys. Oceanogr.* **25**, 1350-1364.

Mikolajewicz, U., Maier-Reimer, E., 1990: Internal secular variability in an ocean general circulation model. *Climate Dyn.* **4,** 145-156.

Nese, J.M., and Dutton, J.A., 1993: Quantifying predictability variations in a low-order ocean-atmosphere model: A dynamical system approach. *J. Atm. Sci.* **6**, 185-204.

Palmer, T.N., 1996: *Predictability of the atmosphere and oceans: From days to decades.* In: Large-scale transport processes in oceans and atmosphere, D.T.A. Anderson and J. Willebrand, eds., NATO ASI Series vol. 44, Springer, pp. 83-155.

Reddy, S.C., 1993: Pseudospectra of Wiener-Hopf integral operators and constant-coefficient differential operators. *J. Integral Eqs. Appl.* **5,** 369-403.

Ruddick, B., and Zhang, L., 1996: Qualitative behaviour and nonoscillation of Stommel's thermohaline box model. *J. Climate* **9,** 2768-2777.

Stommel, H.M., 1961: Thermohaline convection with two stable regimes of flow. *Tellus* **13,** 224-230.

Trefethen, L.N., Trefethen, A.E., Reddy, S.C., and Driscoll, T.A., 1993: Hydrodynamic stability without eigenvalues. *Science* **261,** 578-584.

Tzipermann, E., 1997: Inherently unstable climate behaviour due to weak thermohaline circulation. *Nature* **386,** 592-595.

Weisse, R., Mikolajewicz, U., and Maier-Reimer, E., 1994: Decadal variability of the North Atlantic in an ocean general circulation model. *J. Geophys. Res.* **89**, 12411-12421.

Winton, M., 1997: The effect of cold climate upon North Atlantic Deep Water formation in a simple ocean-atmosphere model. *J. Climate* **10,** 37-51.

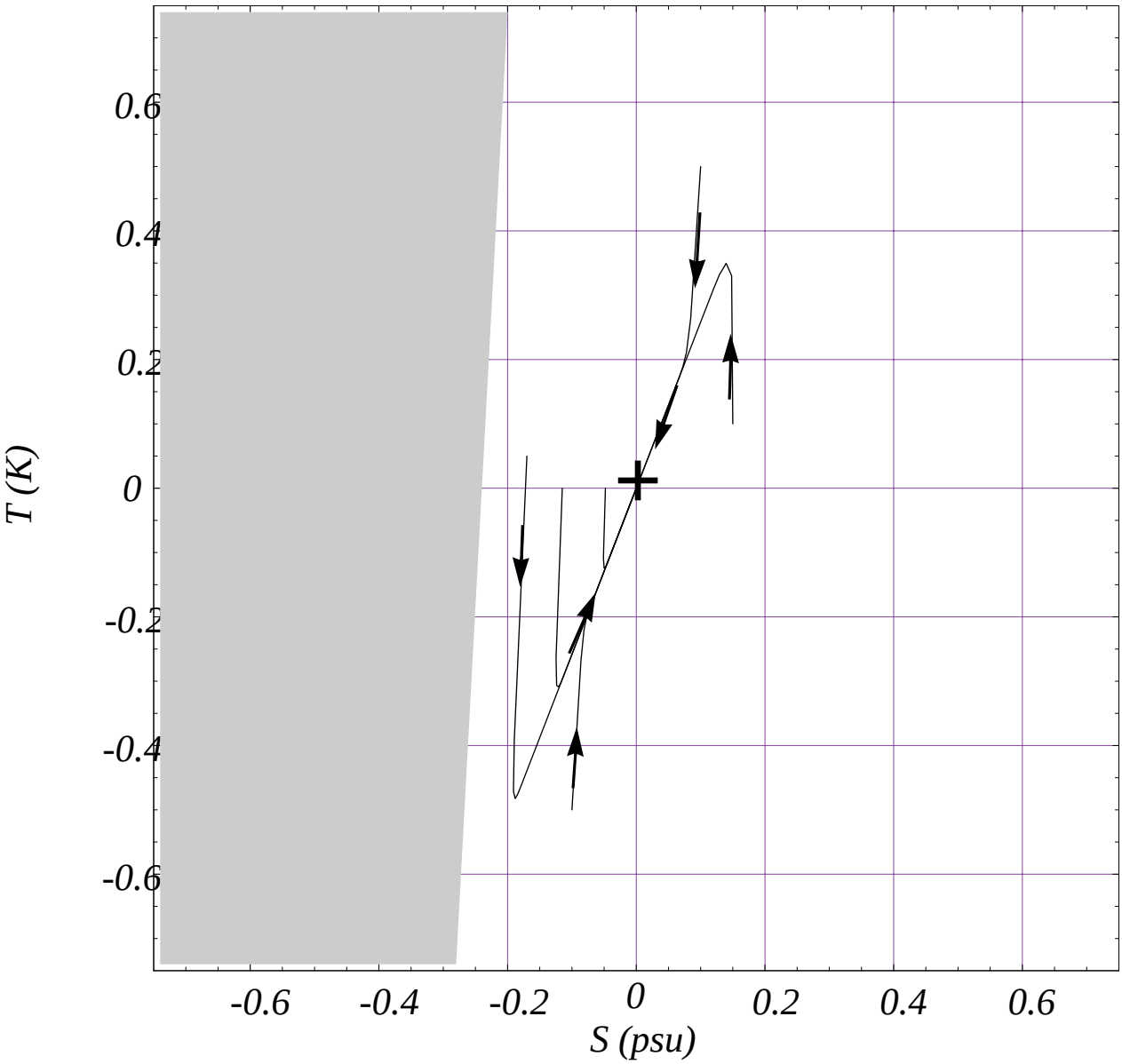

Figure 1: The basin of attraction (white area) and the dynamics in the thermohaline phase space. With initial conditions outside the gray area, the trajectories converge asymptotically to the origin corresponding to the thermal driven solution of the THC. Due to the fast thermal response during the first decade of relaxation, the distance of the trajectories from zero can increase temporarily.

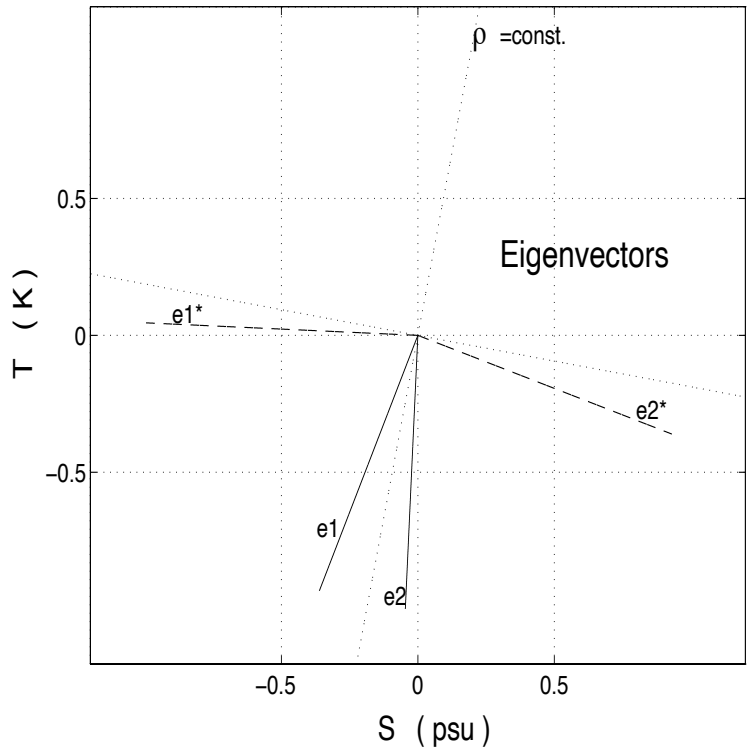

Figure 2: Eigenvectors $\boldsymbol{e}_1, \boldsymbol{e}_2$, and adjoint eigenvectors $\boldsymbol{e}_1^*, \boldsymbol{e}_2^*$ of the tangent linear operator $\boldsymbol{A}$. The dotted lines show the line of constant density and the perpendicular.

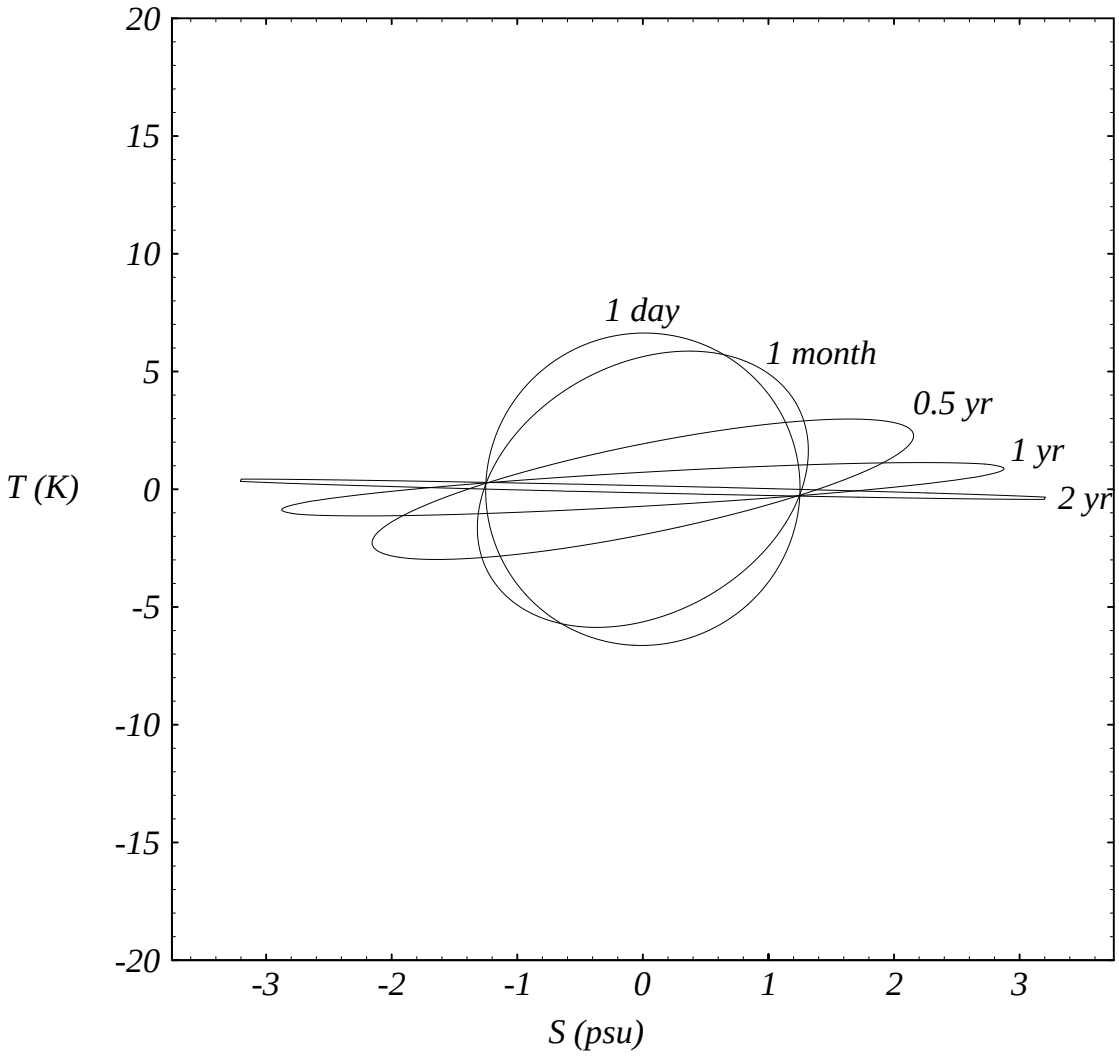

Figure 3: Forecast ellipsoid after 1 day, 1 month, 6 months, 1 year, and 2 years. The main axes of the ellipsoids define the singular vectors of the system. After a year, the dominant singular vector coincides almost with sea surface salinity anomalies. The axes are scaled for equal contributions of salinity and temperature anomalies to high latitude density.

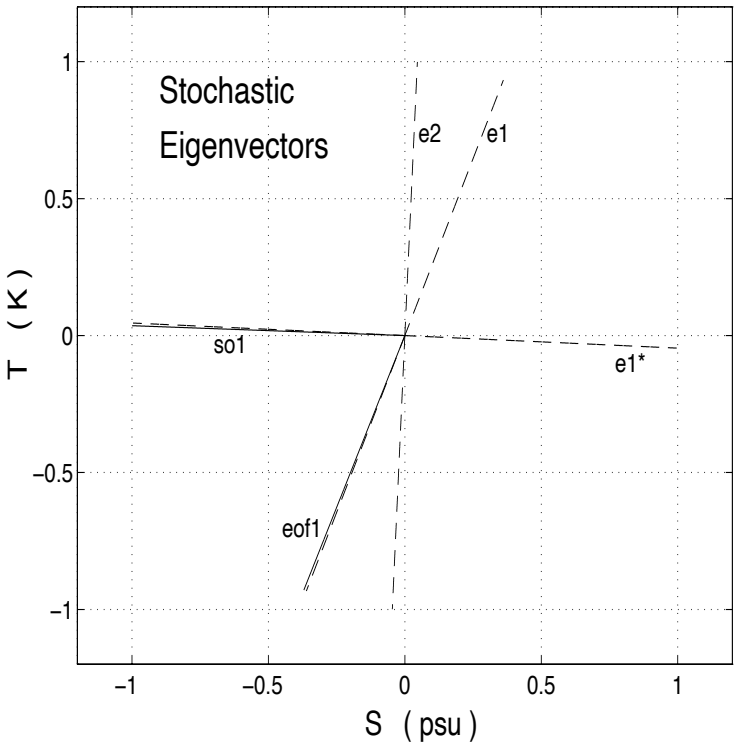

Figure 4: The first EOF (eof1) and the stochastic optimal (so1) in the phase space of temperature and salinity anomalies. For orientation, the eigenvectors $\boldsymbol{e}_1, \boldsymbol{e}_2$ and adjoint eigenvector $\boldsymbol{e}_1^*$ are shown with dashed lines.

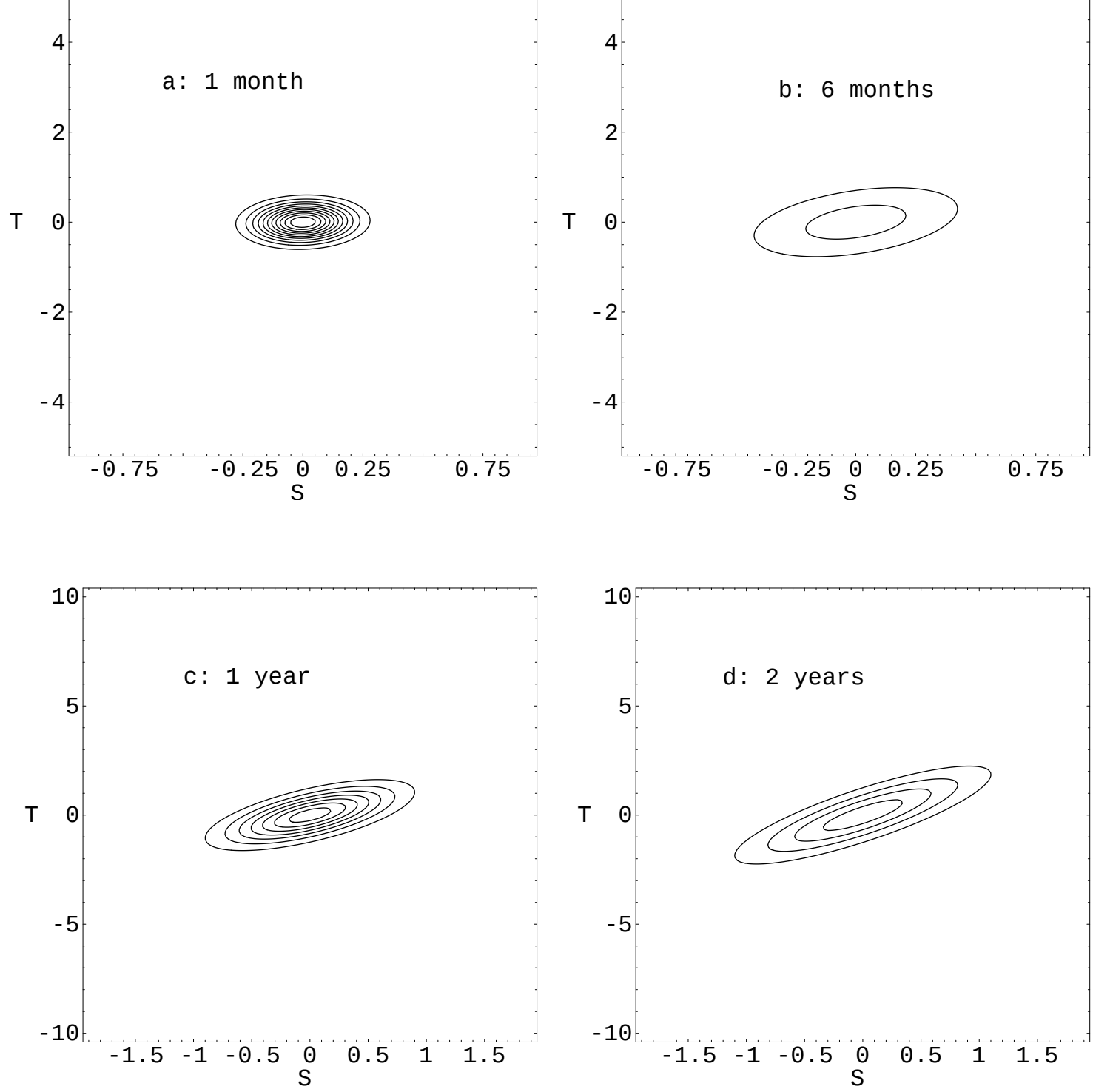

Figure 5: Development of the probability distribution function (PDF). Starting with a $\delta-$function in (0,0), the PDF is shown after one month (a) and 6 months (b) with contour interval 1, and after one year (c) and two years (d) with contour interval 0.2. The axes are scaled for equal contributions of salinity and temperature to high latitude density with units psu and K, respectively.

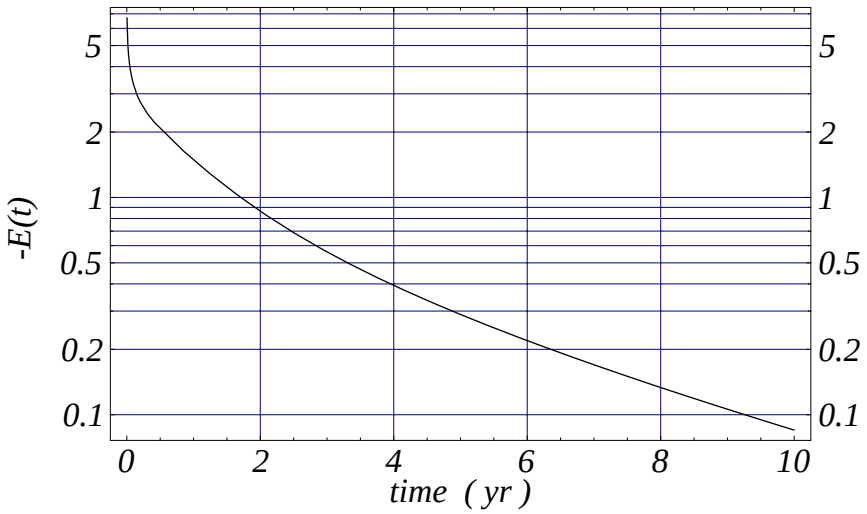

Figure 6: Time evolution of the negative relative entropy which provides a measure for the knowledge about the system. For a description, we refer to section 4.2 and Appendix A.2.